2 Polymer-Particle Filler Systems

2.1 Introduction

In this chapter we consider the characteristics of binary polymer-solid particle suspensions. Our concern is with polymer-particle interaction and particle-particle interactions, especially in their roles to influence the melt flow and enhance solid mechanical behavior. We discuss the behavior of isotropic- and anisotropic-shaped particle compounds in thermoplastics, including rheological behavior from low loadings to high loadings obtained using various instruments.

Many of the fillers used in industry are anisotropic in character. Depending on the shape of fillers, they are subdivided into isotropic particles, flakes, and fibers. Anisotropic particles may take on states of orientation because of flow and packing processes. Whether developed during flow or processing, particle orientation influences phenomena ranging from rheological properties to compound processability in industrial processing equipment, electrical characteristics, and mechanical performance.

2.2 Particle Properties and Interaction

Depending on the physical properties and size of fillers, the behavior of particle-filled suspensions and filled polymer compounds change. Such properties primarily include particle density, shape, and interaction. To these might be added particle hardness, refractive index, thermal conductivity, electrical conductivity, and magnetic properties.

2.2.1 Particle Density

The densities of particles suspended in liquids and solids range from 0.03 to 20 g/cm^3, but most particles have densities that range from 2 to 3 g/cm^3, as shown in Table 2.1. The density of a compound ρ_c is determined by the density of the polymer and the suspended particles. In a uniform particle distribution, the specific volume of a compound (volume per unit mass) may be represented in terms of the volume fractions ϕ_{part} (particles) and ϕ_{matrix} (matrix) of its components and their specific volume $\overline{v}_{\text{part}}$ and $\overline{v}_{\text{matrix}}$:

$$\overline{v}_{\text{c}} = \phi_{\text{part}}\, \overline{v}_{\text{part}} + (1 - \phi_{\text{part}})\, \overline{v}_{\text{matrix}} \tag{2.1a}$$

or equivalently

Table 2.1 Densities of Important Particle Reinforcers Fillers

Particle	Density (g/cm^3)	Particle	Density (g/cm^3)
Expanded polymeric microspheres	0.03–0.13	Clay	2.6
Hollow glass beads	0.12–1.1	Hydrous calcium silicate	2.6
Thin-wall hollow ceramic spheres	0.24	Vermiculite	2.6
Wood flower	0.4–1.35	Quartz and sand	2.65
Porous ceramic spheres	0.6–1.05	Pyrophyllite	2.65–2.85
Silver coated glass beads	0.6–0.8	Aluminum powders and flakes	2.7
Thicker wall hollow ceramic spheres	0.7–0.8	Talc	2.7–2.85
Polyethylene fibers and particles	0.9–0.96	Nickel coated carbon fiber	2.7–3.0
Cellulose fibers	1.0–1.1	Calcium carbonate	2.7–2.9
Unexpanded polymeric spheres	1.05–1.2	Mica	2.74–3.2
Rubber particles	1.1–1.15	Zinc borate	2.8
Expanded perlite	1.2	Beryllium oxide	2.85
Anthractite	1.31–1.47	Dolomite	2.85
Aramid fibers	1.44–1.45	Wollastonite	2.85–2.9
Carbon black	1.7–1.9	Aluminum borate whiskers	2.93
PAN-based carbon fibers	1.76–1.99	Zinc stannate and hydroxy stannate	3.0–3.9
Precipitated silica	1.9–2.1	Silver coated aluminum powder	3.1
Pitch-based carbon fibers	1.9–2.25	Apatite	3.1–3.2
Fumed and fused silica	2.0–2.2	Barium metaborate	3.3
Graphite	2.0–2.25	Titanium dioxide	3.3–4.25
Sepiolite	2.0–2.3	Antimony pentoxide	3.8
Diatomaceous earth	2.0–2.5	Zinc sulfide	4
Fly ash	2.1–2.2	Barium sulfate and barite	4.0–4.9
Slate flour	2.1–2.7	Lithopone	4.2–4.3
PTFE (polytetrafluoroethylene)	2.2	Iron oxides	4.5–5.8
Calcium hydroxide	2.2–2.35	Sodium antimonite	4.8
Silica gel	2.2–2.6	Molybdenum disulfide	4.8–5.0
Boron nitride	2.25	Antimony trioxide	5.2–5.67
Pumice	2.3	Zinc oxide	5.6
Attapulgite trihydroxode	2.4	Nickel powder or flakes	8.9
Magnesium oxide and hydroxide	2.4	Copper powder	8.92
Unexpanded perlite	2.4	Silver coated copper powders + flakes	9.1–9.2
Solid ceramic spheres	2.4–2.5	Molybdenum powder	10.2
Solid glass beads	2.46–2.54	Silver powder and flakes	10.5
Kaolin and calcinated kaolin	2.5–2.63	Gold powder	18.8
Silver coated glass spheres and fibers	2.5–2.8	Tungsten powder	19.35
Glass fibers	2.52–2.68		
Feldspar	2.55–2.76		

$$\frac{1}{\rho} = \frac{\phi_{\text{part}}}{\rho_{\text{part}}} + \frac{1 - \phi_{\text{part}}}{\rho_{\text{matrix}}} \tag{2.1b}$$

where the densities ρ are reciprocals of the specific volumes.

Compound density in products can vary locally due to uneven distribution of fillers. For example, in one study on glass-filled polystyrene in an injection molding process, the density varied between 0.9 and 1.4 g/cm^3, depending on sampling location and process condition in an injection molded bar [1].

2.2.2 Particle Size

The particle sizes of industrially used particulates vary from 50 to 100 μm at the largest level to 0.01 μm (10 nm) on the smallest scale (see Table 2.2). At the largest scale are metallic flakes and powders and some glass beads. The diameters of glass, aramid, cellulosic, and carbon fibers are usually 10 to 12 μm. Mineral fillers, such as calcium carbonate, mica, and talc, are in the range of 0.07 to 5 μm. Titanium dioxide is about 0.1 μm. Carbon black and silica are primarily in the range of 0.01 to 0.05 μm. The smallest mineral particles are silicate layers of fully exfoliated clays (usually montmorillonite).

The size of particles is often discussed in terms of surface area. For spherical particles of diameter d, the area per unit mass of particle $(a = A/M)$ is

$$a = \frac{A_{\text{part}}}{M_{\text{part}}} = \left[\frac{\pi\, d^2}{\rho_{\text{part}} \left(\frac{\pi\, d^3}{6} \right)} \right] = \frac{6}{\rho_{\text{part}}\, d} \tag{2.2}$$

We may also use $\overline{d}$, the average particle diameter, in place of d. This might be defined, based on Eq. 2.2, by

$$\overline{d} = \frac{\sum N_i\, d_i^3}{\sum N_i\, d_i^2} \tag{2.3}$$

Different particle size averages may be defined analogously to the averages used for molecular weights (Eq. 2.1).

Generally, particle surface areas consist of a sum of both external surface area a_{ext} and internal surface area a_{int} with particles. The latter is very important for porous catalyst particles. We may write

$$a = a_{\text{ext}} + a_{\text{int}} \tag{2.4}$$

Table 2.2 Commercial Particle Dimensions

Particle type	Diameter (μm)	BET area (m^2/g)
Aluminum borate whiskers	0.5–1	2.5
Aluminum oxide	13–105	0.3–325
Aluminum trihydroxide	0.7–55	0.1–12
Antimony trioxide	0.2–3	2–13
Attapulgite	0.1–20	120–400
Barium Sulfate	3–30	0.4–31
Barium titanate	0.07–2.7	2.4–8.5
Bentonite	0.18–1	0.8–1.8
Boron nitride	3–200	0.5–25
Calcium carbonate	0.2–30	5–24
Calcium carbonate (precipitated)	0.02–0.4	–
Calcium hydroxide	5	1–6
Carbon black	15–250	10–560
Ceramic beads (hollow)	50–350	0.1–1.1
Ceramic beads (solid)	1–200	
Clay	0.4–5	19–31
Copper	1.5–5	–
Cristobalite (micronized)	0–6	0.4–6.5
Cristobalite (coarse)	0–200	–
Diatomaceous earth	3.7–25	0.7–180
Ferrites	0.05–14	210–6000
Feldspar	3.2–14	0.8–4
Glass beads	7–8	0.4–0.8
Gold	0.8–9	0.05–0.8
Graphite	6–96	6.5–20
Hydrous calcium silicate	9	95–180
Iron oxide	0.8–10	30–60
Kaolin	0.2–7.3	8–65
Lithopone	0.7	3–5
Magnesium hydroxide	0.5–7.7	1–30
Mica	4–70	1.1–2.6
Nickel	2.2–9	0.6–0.7
Perlite	11–37	1.88
Sepiolite (hydrated magnesium silicate)	5–7	240–310
Fumed Silica	5–40	50–400
Fused silica	4–28	0.8–3.5
Precipitated silica	1–40	12–800
Quartz silica (microcrystalline silica, tripoli, novaculite)	2–19	–

Table 2.2 (continued)

Particle type	Diameter (μm)	BET area (m^2/g)
Sand (silica flour, ground silica)	2–90	0.3–6
Silica gel	2–15	40–850
Silver powder and flakes	0.25–25	0.15–6
Talc	1.4–19	2.6–35
Titanium dioxide	8–300	7–162
Wood flour	10–100	55–60 (oil absorption)
Wollastonite	1–50	0.4–5
Walnut shell flour	9.0	0.5
Zeolites	50	–
Zinc borate	0.6–1	10–15
Zinc oxide	0.036–3	10–45
Zinc sulphide	0.3–0.35	8

It is well known to scientists who work with suspensions of particles or polymer-particle compounds that there is a fundamental change in the behavior of particles of these systems as the particle dimensions change. When the particles are large, hydrodynamic effects dominate their flow (rheological) behavior and similar elastic characteristics dominate their modulus and ultimate behavior. When the particle sizes are reduced, the attractive forces between them become increasingly important. The critical dimension distinguishing these two regimes is in the neighborhood of 5 μm but depends upon the particle material.

Researchers [2 to 10] who have studied the rheological properties of suspensions of particles in both Newtonian liquids [2 to 4] and polymer fluids [5 to 10] have long found that the shear viscosity increases as the volume fraction of particles increases. Further, the shear viscosity at constant volume fraction solids increases as the particle size decreases. In addition, the rheological responses become more complex and greater time dependences of stress responses are found as particle size decreases. Yield values, a stress below which there is no flow, develop and increase with both higher particle loading and decreasing particle size [2, 4, 10 to 26]. This was first clearly seen in rubber compounds by Scott [11] as early as 1931. The effects are greater when the interparticle forces are stronger.

2.2.3 Particle Shape

Particles have a range of shapes. Some are roughly spherical. Others are aggregates of covalently bonded spheres (carbon black, silica). Still other widely used particles are flakes (mica, talc, clays) and fibers (cellulose, melt spun glass, synthetic fibers). Particles of the latter type are capable of orienting and forming anisotropic compounds where mechanical, optical, and thermal properties vary with direction. Regions of local order develop in normal isotropic systems of fibers or flakes because of difficulties in packing these particles together.

2.3 Hydrodynamic Theory of Suspensions

2.3.1 General

In the first decade of the 20th century, Einstein [27] gave his attention to the prediction of the viscosity of a dilute suspension of spheres. Einstein began with the creeping flow Navier-Stokes equation of Newtonian fluid hydrodynamics:

$$0 = -\nabla p + \eta \, \nabla^2 \underline{v} \tag{2.5a}$$

The fluid was considered to adhere to the surface of the sphere

$$\underline{v}\,(R, \theta, \phi) = 0 \tag{2.5b}$$

Here $\underline{v}$ is velocity, p is pressure, η is viscosity, and R is the radius of the sphere.

Stokes [28] had earlier used Eq. 2.5 for analyzing the flow around a sphere. Einstein argued that the viscosity of the suspension could be determined by the increase of the energy dissipated, Φ, by the presence of the sphere, i.e.,

$$\frac{\eta}{\eta_0} = \frac{\Phi}{\Phi_0} = \frac{\oint \underline{\sigma} \cdot \underline{v} \cdot n \, d \, a}{\oint \underline{\sigma}^{(0)} \cdot \underline{v}^{(0)} \cdot \underline{n} \, d \, a} \tag{2.6}$$

where $\underline{\sigma}$ is the stress tensor, $\underline{n}$ is a unit normal to the surface 'a' of the suspended sphere; η_0 is the viscosity of the suspending medium and $\underline{\sigma}^{(0)}$ and $\underline{v}^{(0)}$ the stress and velocity fields in the absence of the sphere. He was able to show that the viscosity, at very low volume fractions of spheres, increased according to

$$\frac{\eta}{\eta_0} = 1 + 2.5 \, \phi \tag{2.7}$$

where ϕ is the volume fraction of the spheres. Eq. 2.7 is valid only for extremely dilute suspensions, in which interactions between neighboring particles are negligible (i.e., in the absence of hydrodynamic interactions). The method of Eq. 2.6, however, can also be applied to more concentrated systems of suspended particles.

In 1945 Guth [29] noted the similarity of the mathematical formulations of the theory of linear elasticity with those of Newtonian fluid hydrodynamics. He saw that if the elastic solid were incompressible that the presence of rigid spheres would similarly increase the modulus G according to elastic energy arguments, specifically,

$$\frac{G}{G_0} = \frac{W}{W_0} = \frac{\oint \underline{\sigma} \cdot \underline{\varepsilon} \cdot \underline{n} \, d \, a}{\oint \underline{\sigma}^{(0)} \cdot \underline{\varepsilon}^{(0)} \cdot \underline{n} \, d \, a} \tag{2.8}$$

where W is the elastic strain energy, $\underline{\varepsilon}$ is the infinitesimal strain and G_0 is the modulus of the suspending medium and $\underline{\sigma}^{(0)}$ and $\underline{\varepsilon}^{(0)}$, the stress and strain field in the absence of the sphere. This leads to for dilute systems of spheres to

$$\frac{G}{G_0} = 1 + 2.5\,\phi \tag{2.9}$$

which is the same as Einstein's Eq. 2.7.

2.3.2 Spheres

The formulation described above is found to be valid for large particles about 10 μm or greater. It does not consider van der Waals and dipole-dipole forces between particles. It is, as we will see, able to consider concentration effects and the influence of particle anisotropy.

The effect of concentration on viscosity of suspensions of spheres was first modeled by Guth and Simha [30]. They again began with Eq. 2.5, but considered the hydrodynamic interaction of other spheres on the velocity field. This led to an enhancement of the viscous dissipation and to an increase in suspension viscosity of form

$$\frac{\eta}{\eta_0} = 1 + 2.5\,\phi + C\,\phi^2 \tag{2.10}$$

The value of C has been variously given as 14.1 and 12.6 [30, 31].

It follows from the previously mentioned arguments of Guth [29] that the elastic modulus for an incompressible solid should be equivalently given by

$$\frac{G}{G_0} = 1 + 2.5\,\phi + C\,\phi^2 \tag{2.11}$$

Studies of the viscosity of suspensions at higher concentrations have usually used cell models. Here, one essentially considers the spheres are arranged in a lattice-like array, and one analyzes the flow in a representative cell. Cell models are critically discussed in the monograph of Happel and Brenner [32]. Such an approach was initiated by Simha [33]. He analyzed the flow around a sphere located in a cell. He predicted

$$\frac{\eta(\phi)}{\eta_0} = 1 + 5.5\,\Psi(\phi)\cdot\phi \tag{2.12}$$

where ϕ is volume fraction and $\Psi(\phi)$ is a concentration dependent interaction parameter. When ν is small, $\Psi(\phi)$ is equal to unity. Thus Simha's formulation does not reduce to Einstein's Eq. 2.7. Variant cell theories of concentrated suspension of spheres in Newtonian fluids have been developed by Happel [34], and Frankel and Acrivos [35].

Tanaka and White [36] using the Frankel-Acrivos cell theory formulation have modeled the shear flow of a concentrated suspension of spheres in a power law non-Newtonian fluid (Eq. 2.5b).

Mooney [37] has developed a formulation of the viscosity of suspensions of spheres based on a functional equation, which must be satisfied if the final viscosity is to be independent of the sequence of stepwise additions of partial volume fractions of the spheres to the suspension. Further Einstein's Eq. 2.7 is considered valid for dilute suspensions, Mooney argues for a monodisperse system of spheres that

$$\frac{\eta}{\eta_0} = \exp\left[\frac{2.5\,\phi}{1 - k\,\phi}\right] \tag{2.13}$$

where k is a self-crowding factor. The parameter k was found experimentally to be between 1.35 and 1.91.

2.3.3 Ellipsoids

In 1922 G. B. Jeffery [38] sought to generalize Einstein's analysis for a dilute suspension of spheres to ellipsoids. Like Einstein [27], he considered the sphere to be in shear flow $\underline{v}_1^{(0)} = \dot{\gamma}\, x_2$, $v_2^{(0)} = v_3^{(0)} = 0$. The flow creates stresses at the surface, which causes rotation as well as a translation of the ellipsoid. During shear flow, the particles undergo motions involving regular orbits, which have become known as Jeffery orbits. The long axes of prolate and oblate particles are immersed in a fluid in laminar motion. They will tend to set themselves parallel to the flow direction. Using the creeping flow Navier-Stokes equations, he found the stresses at the ellipsoid surface are equivalent to the sum of two couples. One tends to make an elongated particle (prolate ellipsoid of revolution) adopt the same rotation as the undisturbed flow. This makes the particle axis tend to lie parallel to the 3 direction and adopt the same rotation as the flow field. The other tends to make an elongated particle rotate in the 1-2 plane.

Jeffery [38] predicted that the viscosity of a very dilute suspension of ellipsoids in a shear field of Newtonian liquid would have the form

$$\frac{\eta}{\eta_0} = 1 + \overline{\nu}\,\phi \tag{2.14}$$

where $\overline{\nu}$ is a parameter which depends on the aspect ratio and orientation of the ellipsoidal particles. For spheres it is 2.5. Jeffery found that $\overline{\nu}$ varies from 2.0 to very large values for prolate spheroids, which approach rods.

A major significance of Jeffery's studies lies in the derivation of equations of anisotropic particle motion in a Newtonian liquid. He predicted that shear flow rotates the disc/rod in shear planes. Jeffery hypothesized that in time the orbital motions would evolve to the one that corresponds to the least viscous dissipation. The motion of single ellipsoids in the shear

flow of water has been investigated experimentally by Taylor [39, 40]. Particle orbits in the flow of dilute suspensions of ellipsoids have also been observed by Mason and coworkers [41 to 44]. We discuss this in Section 2.4.2.1.

There are no equivalent studies of concentrated anisotropic suspensions. This is because of the tendency of anisotropic particles to form oriented ordered structures such as "micro-bundles" of fibers. Batchelor [45] has modeled the flow of concentrated suspensions of large parallel fibers. Very large elongational viscosities are predicted. This was extended to suspensions in non-Newtonian fluids by Goddard [46].

2.3.4 Interacting Particles

We may modify the above approaches to include interparticle forces. It is possible in this way to predict the non-Newtonian responses due to interparticle forces and yield values. These may be incorporated into cell models of suspensions. An early study of this was by Tanaka and White [36] using a power law fluid matrix.

2.3.5 Continuum Theories

Continuum mechanics theories of various types have been developed through the years to represent the flow of suspensions. The earliest efforts of this type were one-dimensional, but from the 1940s there have been three-dimensional efforts, which we will emphasize here.

Scott [11] in a 1931 study, one of the earliest studies of the rheology of rubber compounds for these materials, suggested combining a yield value, Y, and a power law

$$\sigma = Y + K\,\dot{\gamma}^n \tag{2.15}$$

for shear flow. Here σ is a shear stress, n the power law exponent, and K, a coefficient. Expressions of this type were widely used in succeeding years to model the flow of suspensions.

In papers published in 1947 and 1948, Oldroyd [47] developed a three-dimensional of Eq. 2.15 that could predict non-Newtonian viscosity and three-dimensional "plastic" yielding based on a von Mises stress criterion. Subsequently, Slibar and Pasley [48] developed a similar three-dimensional model, which accounted for thixotropy.

In 1979 White [49] proposed a three-dimensional theory of a plastic-viscoelastic fluid intended to represent the behavior of small particle-filled compounds. This was also based on the von Mises stress criterion but contained memory and predicted shear flow normal stresses. This was later generalized to include thixotropy [50, 51]. Leonov [52] developed an alternative three-dimensional tensor theory of this behavior.

In more recent years, White and Suh [53] and White et al. [54] have developed three-dimensional models of compounds with anisotropic disklike particles, which exhibit yield values. These produce direction dependent flow characteristics. Later Robinson et al. [55] described a transversely isotropic Bingham fluid model.

2.4 Experimental Studies of Compound Properties

2.4.1 Large Spheres

The viscosities of suspensions of large non-interactive spheres have been made by various investigators [56 to 60]. The agreement of experimental data with the hydrodynamic theory seems not clear in either dilute or concentrated systems. The best correlation of data with a model over wide range concentrations is with Mooney's [36] Eq. 2.13.

At very high concentrations, Reynolds [61] called attention to the possibility of a phenomenon he called "dilatancy" occurring. By this he meant that shear flow would induce an expansion of the suspension during flow. This is caused by the break up the lattice like structure, which might develop at rest in a concentrated suspension of spheres. Subsequently, Freundlich and Roder [62] presented arguments in 1938 that Reynolds dilatancy would involve not only a dilation of the suspension but also an increase in the shear viscosity.

In subsequent years, various investigators searched for the Reynolds [61] and Freundlich-Roder [62] effects in concentrated suspensions of small particles. Of special interest are the researches of Metzner and Whitlock [63] and Hoffmann [64]. The former authors [63] described experiments on a titanium dioxide particle suspension of unspecified particle size and suspensions of large glass spheres (28 to 100 μm). Both volumetric dilation and Freundlich-Roder viscosity increases were only observed in the titanium dioxide suspensions, but appeared to occur independently with volumetric dilation occurring at lower shear stresses/rates.

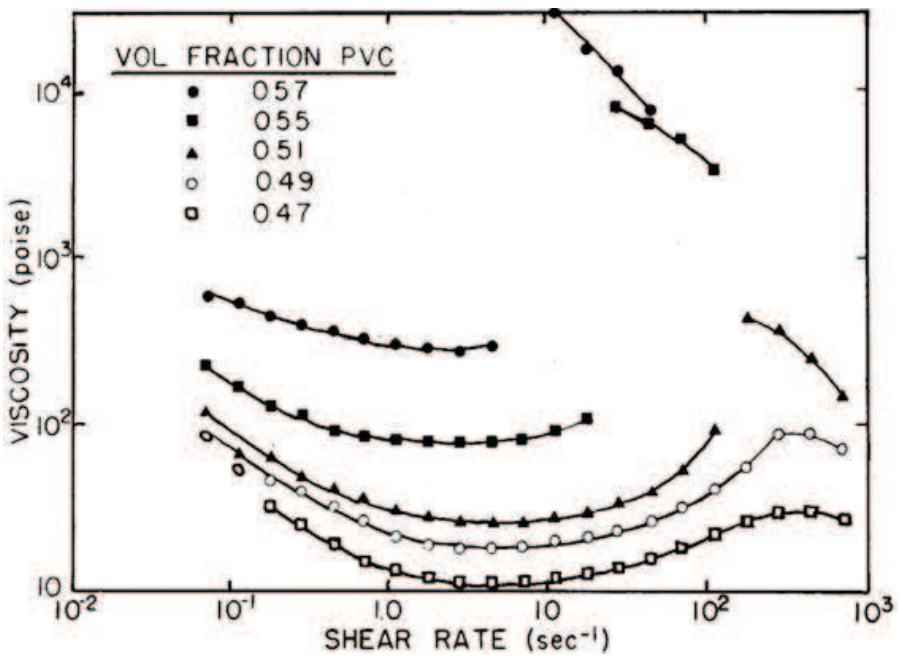

Figure 2.1 Hoffman's [64] study of the viscosity of suspension of polyvinyl chloride particles

Hoffman [64] studied monodisperse suspensions of polyvinyl chloride and styrene-acrylonitrile copolymer particles of diameter 0.4 to 1.25 μm using both rheological and structural characterization techniques as shown in Figure 2.1. The shear viscosities showed striking viscosity increases at critical shear rates. Structurally, the suspensions at low shear rates were found to exhibit a hexagonal crystalline lattice. At a critical shear rate, this lattice structure broke up into less-oriented arrays with a jump increase in shear viscosity.

There are few studies of suspensions of large particles in polymer melts. Nazem and Hill [65] investigated the influence of glass spheres of diameter 10 to 60 μm on melt viscosity in a styrene-acrylonitrile copolymer (SAN) matrix. Generally, the viscosity is increased by the presence of the spheres. The general shape of the viscosity-shear rate curves was unchanged.

2.4.2 Large Fibers and Ellipsoids

2.4.2.1 Fluids

As noted earlier, in the 1920s Taylor [38] experimentally verified Jeffery's [37] analysis for the motion of ellipsoids. There were subsequent studies by Taylor in the 1930s [39, 40]. In the 1950s Mason and his coworkers [41 to 44] made extensive efforts to visualize anisotropic particle motions in dilute suspensions during flow of rigid rod- and disk-shaped particles. They observed a distribution of orbits.

There is a significant literature beginning in the 1970s [66 to 73] on the flow of glass fiber suspensions in both Newtonian fluids and in polymer melt matrices. This literature describes rheological properties including the shear viscosity, normal stresses, and elongational flow characteristics. It also includes the development of fiber orientation in flow and fiber breakage. These fibers were of order 10 to 12 μm in diameter, and there are only very weak attraction forces.

Maschmeyer and Hill [69] describe experimental studies of glass fibers suspended in silicone oil. There were great problems associated with reproducibility, fiber breakage, and clogging of capillary die entries. Most striking was their observation of Weissenberg normal stress effects (i.e., rod climbing by the suspension when stirred). Normal stress effects, as discussed in Section 1.3.5, are commonly found in polymer solutions. It is surprising at first, but on later consideration instructive, to see them in fiber suspensions in a Newtonian liquid.

The first extensive experimental investigation on the rheological properties of glass fiber-polymer melt suspensions was by Chan et al. [70 to 72]. They investigated polymer melt compounds of polyethylene, polystyrene, and isotactic polypropylene. These authors found that the fibers enhanced the shear viscosity of melts, but did not induce yield values (see Fig. 2.2). The compound exhibited very large normal stresses and a high elongational viscosity (see Fig. 2.3). A subsequent paper by Czarnecki and White [73] confirmed these observations on the shear viscosity and normal stresses in polystyrene compounds. This paper also makes comparisons with aramid and cellulosic fibers, whose suspensions in polymer melts have similar behavior. They showed that masticating glass fiber compounds damages and breaks fibers. It was found that this reduces the normal stresses (Fig. 2.4).

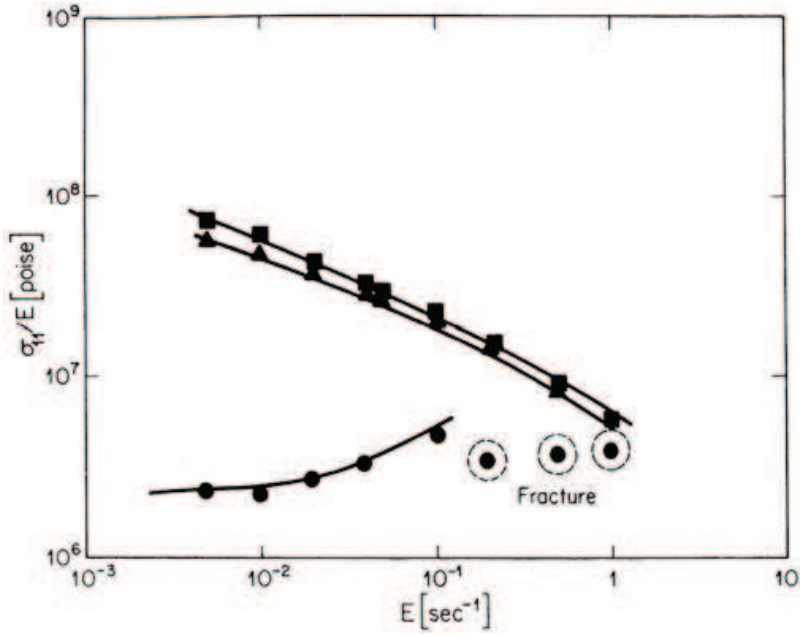

Figure 2.2 Elongational viscosity of a suspension of a suspension of glass fiber ($\phi = 0.2$ (▲) and 0.4 (■)) in a polystyrene melt (Chan et al. [70])

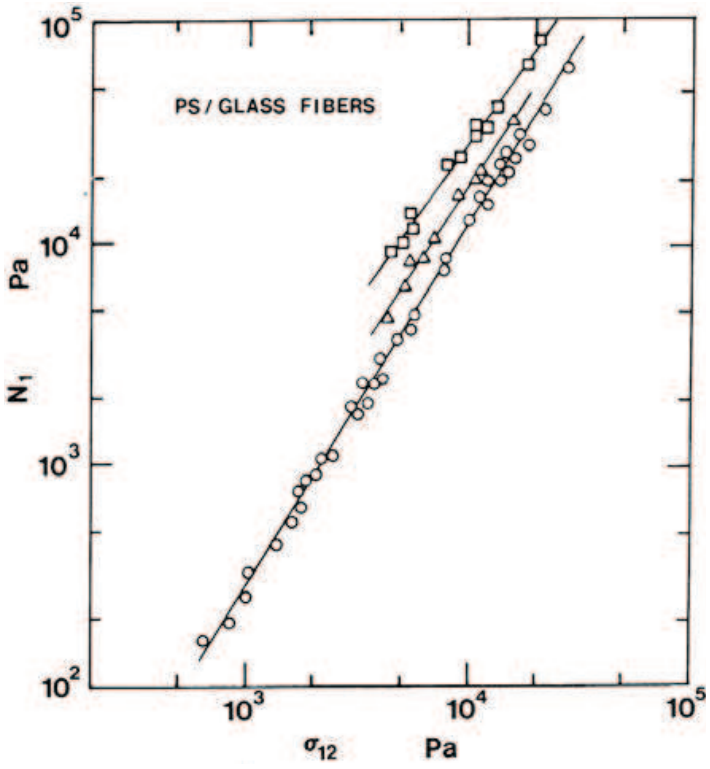

Figure 2.3 Principal normal stress difference N_1 vs. shear stress with 0 (○), 10 (△), and 22 (□) vol% glass fibers (Chan et al. [70])

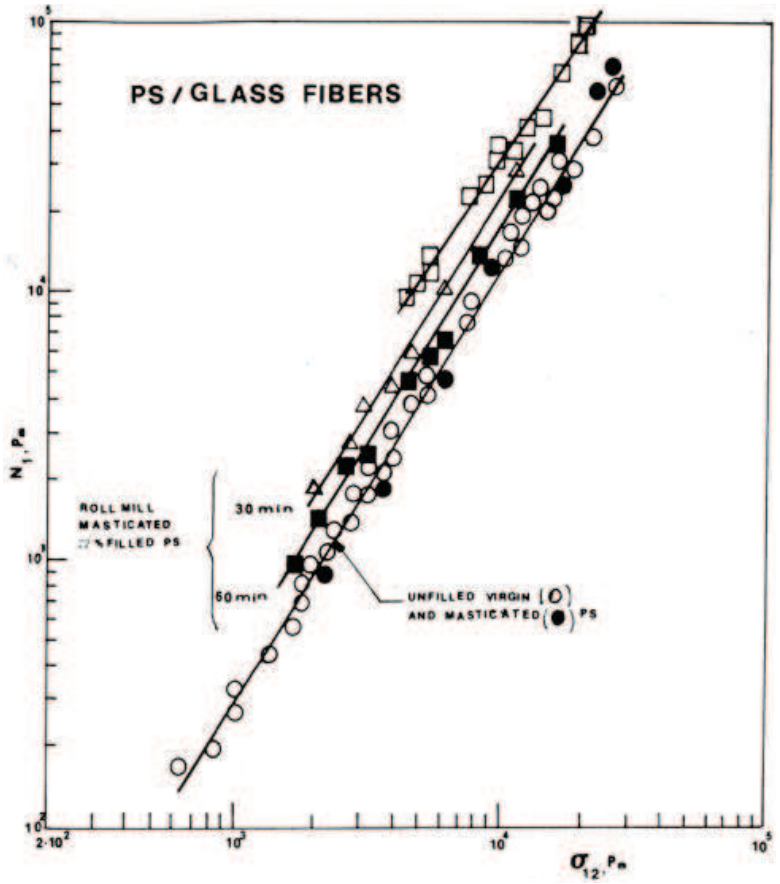

Figure 2.4 Principal normal stress difference N_1, as function of shear stress σ_{12} for a polystyrene melt and 22 (□) volume percent glass fibers before mastication and after 30 and 60 min mastication (Czarnecki and White [73])

O'Connor [74] was the first to compare breakage of different reinforcing fibers during mixing. Czarnecki and White [73] compared the breakage of aramid and cellulose fibers with glass fibers. Glass fibers become severely damaged rapidly. Both aramid and especially cellulose fibers break more slowly. The aramid fibers broke into a segmented structure. The cellulose fibers are annular cylinders that have collapsed and buckled (Section 1.4.12.1). With their resulting helical shape, they are much more flexible and did not similarly break.

Extensive studies of glass fiber damage in continuous mixers have in more recent years been described by Franzen et al. [75] and by Shon and White [76].

Forgacs and Mason [77] and later Czarnecki and White [73] investigated the mechanisms of fiber breakage during flow and concluded that it was associated with Euler buckling of the filaments in shear flows.

2.4.2.2 Solids

High modulus continuous filament fibers significantly enhance the Young's modulus and tensile strength of polymers. This is illustrated by a simple derivation. If the fibers are all

parallel, the strain of the fibers and matrix must be the same in a mechanical test. The applied force is

$$F = [A_f\ E_f + A_m\ E_m]\,\gamma = A_c\ E_c^{II}\ \gamma \tag{2.16a}$$

where E_f and E_m are the modulus of fiber and matrix and A_f and A_m are the cross-section of fiber and matrix, E_c^{II} is the composite modulus parallel to the fibers. This leads to the composite modulus [78],

$$E_c^{II} = \phi_f\ E_f + (1 - \phi_f)\,E_m \tag{2.16b}$$

where ϕ_f is the volume fraction of fibers taken as A_f / A_c. Clearly, E_f quickly overwhelms E_m as ϕ_f increases.

The above behavior is not found when the continuous filaments are perpendicular to the direction of stretch. Consider the perpendicular modulus $E^{\perp}$ here the deformation of matrix and fibers are additive. Let $\delta\, l_c$ be the deformation of the composite, $\delta\, l_f$ that of the fibers and $\delta\, l_m$ that of the matrix.

$$\delta\, l_c = \phi_f\ \delta\, l_f + \phi_m\ \delta\, l_m \tag{2.17a}$$

This lead to [78]

$$\frac{1}{E_c^{\perp}} = \frac{\phi_f}{E_f} + \frac{\phi_m}{E_m} \tag{2.17b}$$

The orientation of chopped fibers developed during flow/processing can strongly influence various properties of compounds, such as modulus and tensile strength. In 1974 Brody and Ward [79] described fiber orientation in uniaxial fiber filled composites using Hermans orientation factors [80 to 82] originally developed to measure polymer chain orientation in man-made fibers (see Fig. 2.5(a)).

$$f = \frac{3\,\overline{\cos^2\phi} - 1}{2} \tag{2.18}$$

where ϕ is the angle between the fiber axis and the preferred symmetry direction. Subsequently White and Knutssen [83] generalized these considerations to biaxial orientation of fibers. They used the biaxial orientation factors [84]

$$f_1^B = 2\,\overline{\cos^2\phi_1} + \overline{\cos^2\phi_2} - 1 \tag{2.19a}$$

$$f_2^B = 2\,\overline{\cos^2\phi_2} + \overline{\cos^2\phi_1} - 1 \tag{2.19b}$$

where 1 and 2 now represent two orthogonal directions and angles ϕ_1 and ϕ_2 are the angles between these directions (see Fig. 2.5(b)). These orientation factors were originally developed by White and Spruiell [84] to represent biaxial molecular orientation in polymers. Eqs. 2.18 and 2.19a,b are equal to (0,0) for isotropic random orientation. For perfect uniaxial orientation they are equal to (1,0) or (0,1). For equal biaxial orientation in a plane they are (1/2,1/2).